Supplementary Material for "Electronic Transport in Graphene with Aggregated Hydrogen Adatoms"

Fernando Gargiulo,[1] Gabriel Autès,[1] Naunidh Virk,[1] Stefan Barthel,[2,3]
Malte Rösner,[2,3] Lisa R. M. Toller,[1] Tim O. Wehling,[2,3] and Oleg V. Yazyev[1]

[1] *Institute of Theoretical Physics, Ecole Polytechnique Fédérale de Lausanne (EPFL), CH-1015 Lausanne, Switzerland*
[2] *Institut für Theoretische Physik, Universität Bremen, Otto-Hahn-Allee 1, D-28359 Bremen, Germany*
[3] *Bremen Center for Computational Materials Science, Am Fallturm 1a, D-28359 Bremen, Germany*

A. First-principles calculations of the energies of hydrogen adatom clusters

First-principles calculations of the interaction energies of hydrogen adatoms on graphene have been performed within the density functional theory (DFT) framework employing the generalized gradient approximation (GGA) to the exchange-correlation functional [1]. Ultrasoft pseudopotentials [2] for carbon and hydrogen atoms have been used in combination with a plane-wave basis set with a kinetic energy cutoff of 30 Ry for the wavefunctions. Models of hydrogen adatom clusters are based on a graphene 6×6 supercell with 15 Å of vacuum separating the periodic replicas. We used a $2\times2\times1$ Monkhorst-Pack k-point mesh for the Brillouin zone integration [3]. All hydrogen adatom cluster models were relaxed until a maximum force of 0.15 eV/Å on individual atoms was reached. We verified that the chosen parameters provide sufficiently accurate total energies. All calculations have been performed using the PWSCF code of the QUANTUM ESPRESSO package [4].

The interaction energy of a cluster of hydrogen adatoms calculated from first principles E_{DFT} is defined as

$$E_{\mathrm{DFT}} = E_{\mathrm{gr}+n\mathrm{H}} - E_{\mathrm{gr}} - n\,(E_{\mathrm{gr}+\mathrm{H}} - E_{\mathrm{gr}})\,, \tag{1}$$

where $E_{\mathrm{gr}+n\mathrm{H}}$, E_{gr} and $E_{\mathrm{gr}+\mathrm{H}}$ are the total energies of graphene with a cluster of n hydrogen adatoms, pristine graphene and graphene with a single hydrogen adatom, respectively.

In the main text of our manuscript we focused on the situation where hydrogen adatoms are deposited on a single side of graphene. The values of the fitted parameters in expr. (1) of the main text are $\gamma_1 = -1.182$ eV and $\gamma_2 = 0.484$ eV. This scenario is relevant to the case of graphene on a substrate, however in the situation of suspended graphene both sides of graphene are available for binding adatoms. We investigated this situation by studying the same set of adatom clusters as shown in Fig. 1(b) of the main text, but with adatoms placed on the opposite sides of graphene sheet when functionalized carbon atoms belong to different sublattices. The fitted interaction parameters are $\gamma_1 = -1.461$ eV and $\gamma_2 = 0.342$ eV. The excellent agreement between the estimated interaction energies $\tilde{E}$ and the first-principles values E_{DFT} is illustrated in Fig. S1(a). This case is characterized by a stronger attractive

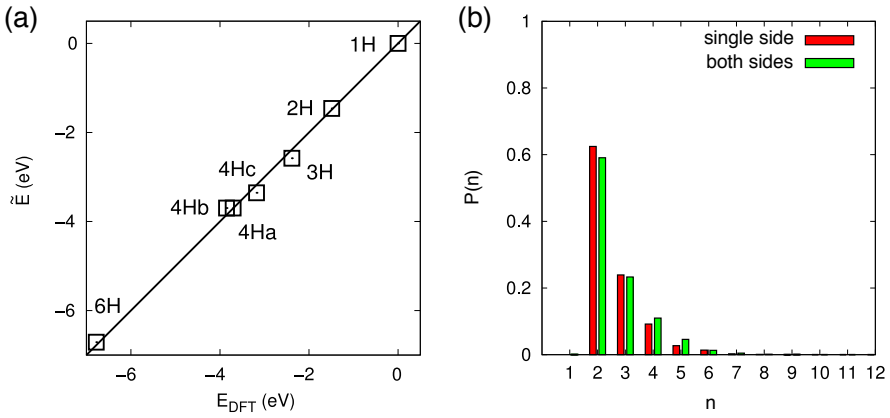

Figure S1: (Color online) (a) Predicted energy $\tilde{E}$ of aggregation of hydrogen adatoms as a function of aggregation energy E_{DFT} calculated from first principles for the set of small clusters shown in Fig. 1(b) of the main text with adatoms adsorbed on both sides of graphene. (b) Comparison of the cluster size distributions $P(n)$ for the cases of single-side and both-sides adatom adsorption at $x = 5\%$ concentration and $T = 300$ K.

contribution and a weaker repulsion compared to the single-side adsorption, thus reflecting the known tendency of forming more stable adatom aggregates upon adsorption on both sides [5, 6]. The cluster size distributions $P(n)$ calculated for single-side and both-sides adsorption at adatom concentration $x = 5\%$ and $T = 300$ K are compared in Fig. S1(b). While the distributions are qualitatively very similar, one notes that both-sides adsorption exhibits a somewhat stronger tendency to form larger clusters.

B. Monte-Carlo simulations of the hydrogen adatoms aggregation

We performed Monte-Carlo simulations with an elementary trial move being the displacement of a randomly chosen adatom to a random carbon atom not populated by another adatom. This move insures the fulfillment of detailed balance. The Metropolis algorithm has been employed for the acceptance/rejection criterion. Once a move has been performed, the system is updated from the old configuration $S_{\rm old}$ to the new one $S_{\rm new}$ with a probability

$$P(S_{\rm old} \to S_{\rm new}) = \min(1, e^{-\beta[\tilde{E}(S_{\rm new})-\tilde{E}(S_{\rm old})]}), \tag{2}$$

where β is the inverse temperature $1/(k_{\rm B}T)$. In all our simulations $T = 300$ K. The number of equilibration steps $N_{\rm eq}$ disregarded from statistical sampling varied between 10^6 and 1.6×10^7, depending on adatom concentration (larger concentrations need more equilibration steps). The total number of steps in our simulations varied between 10^7 and 3×10^7. The equilibration efficacy of our simulation was tested by comparing certain equilibrium properties such as the total energy and cluster size distribution. The properties obtained from Monte-Carlo simulations performed with and without temperature annealing show negligible differences.

C. Landauer-Büttiker electronic transport calculations and scaling analysis of conductivity

In order to investigate the transport properties of graphene with resonant scattering impurities we perform Landauer-Büttiker calculations in a two-terminal configuration with a scattering region composed of hydrogenated

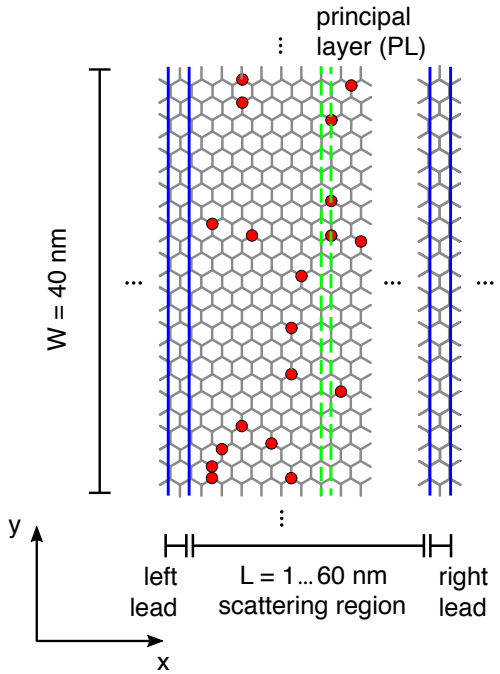

Figure S2: (Color online) Schematic drawing of the two-terminal configuration employed for investigating the transport properties of graphene with hydrogen adatoms. The transport direction is along the x axis while the system is periodic along the y axis. The periodicity along the y axis is $W = 40$ nm. The unit cells of the left and right leads composed of pristine graphene are indicated by blue lines. The scattering region is populated by adatoms either randomly or according to the configurations produced by Monte-Carlo simulations in the case of correlated adatom distributions. One of the principal layers (PL) in the scattering region is indicated by means of green dashed lines.

graphene attached to two semi-infinite leads of pristine graphene, as shown in Fig. S2. The overall configuration is periodic along the transverse direction y. For such a setup, conductance as a function of energy $G(E)$ is given by

$$G(E) = \frac{W}{2\pi} \int_{-\frac{\pi}{W}}^{\frac{\pi}{W}} T(E, k_{\parallel}) dk_{\parallel}, \tag{3}$$

where $T(E, k_{\parallel})$ is the transmission probability and $k_{\parallel}$ is the momentum along y [7]. Due to the large width $W = 40$ nm of the model employed, transmission is only evaluated at the Γ point ($k_{\parallel} = 0$).

In order to calculate $T(E)$ we decompose the scattering region into principal layers (PLs), that is, the layers in which the atoms are coupled at most to those located in the next layer. Since our tight-binding model is limited to first-nearest-neighbor interactions and the transport direction is oriented along zig-zag direction [see Fig. S2], the minimal width of the PL is $d_{\mathrm{PL}} = \frac{\sqrt{3}}{2} d_{\mathrm{CC}}$, where $d_{\mathrm{CC}} = 1.42$ Å is the carbon-carbon bond length. The Hamiltonian restricted to the i-th principal layer is H_i, while t_i is the tight-binding hopping matrix connecting i-th and $i+1$-th principal layers. We introduce an imaginary cleavage plane between the n-th and $n+1$-th principal layers dividing the system into two independent parts. We define g_n^{L} and g_{n+1}^{R} as the surface Green's functions of the two non-interacting semi-infinite systems located on the left and on the right sides of this cleavage plane, respectively.

Following Ref. 8, the transmission is given by

$$T(E) = \mathrm{Tr}[T_n Im(g_n^{\mathrm{L}}) T_n^{\dagger} Im(g_{n+1}^{\mathrm{R}})], \tag{4}$$

where operator T_n is defined as

$$T_n = t_n (1 - g_{n+1}^{\mathrm{R}} t_n^{\dagger} g_n^{\mathrm{L}} t_n)^{-1}. \tag{5}$$

The choice of the position of the cleavage plane is immaterial because of current conservation.

Surface Green's functions g_n^{L} and g_n^{R} can be related to the preceding (successive) surface Green's functions g_{n-1}^{L} (g_{n+1}^{R}) by applying the Dyson equations [9]

$$g_n^{\mathrm{L}} = (E - H_n - t_{n-1}^{\dagger} g_{n-1}^{\mathrm{L}} t_{n-1})^{-1} \tag{6}$$

and

$$g_n^{\mathrm{R}} = (E - H_n - t_n g_{n+1}^{\mathrm{R}} t_n^{\dagger})^{-1}. \tag{7}$$

Further iterations of Eqns. (6) and (7) reduce the problem to the knowledge of the Green's functions at the surfaces separating the scattering region from the left and right leads, g^{LL} and g^{RL}, that we calculated according to the analytic closed form solution described in Ref. 10.

The time complexity of the Green's function calculation for each lead with respect to the number N_{lead} of orbitals in the lead unit cell is $O(N_{\mathrm{lead}}^3)$ [9]. On the other hand, as follows from Eqns. (6) and (7), the complexity of the addition of the layers required to reach the cleavage plane is $O(M \times N_{\mathrm{layer}}^3)$, where M and N_{layer} are the number of principal layers and the number of orbitals in each layer, respectively. Consequently, the overall complexity of the method is cubic with respect to the width and linear with respect to the length of the system.

In order to perform our conductance scaling analysis we vary the length of the scattering region in the range $L = 1...60$ nm by steps of 8 PLs, which corresponds to $\Delta L \approx 1$ nm. At each step the right lead is moved rightwards whereas the left lead is kept fixed [Fig. S2]. The values of conductance $G(E)$ are averaged over an ensemble of N_{ens}=9600 disorder realizations for proper statistical sampling.

D. Complete account of the results of calculations of conductivity and localization length

Conductivity g for the entire investigated range of concentrations is presented in Fig. S3(a,b). The overall enhancement of conductivity upon the aggregation of adatoms is a common feature at all investigated concentrations. This is particularly visible in the strong localization regime, that is at low energies E and large scattering region lengths L. Localization length ξ_{loc} can only be determined for the $g(L)$ curves which exhibit a well-defined negative slope in the large length region. This is the case for $\xi_{\mathrm{loc}} < 60$ nm, which is the maximum scattering region length considered in our study. This does not imply that the system does not undergo localization, but rather that a longer scattering region is needed in order to estimate ξ_{loc} correctly. For this reason many values of localization length ξ_{loc} at $x < 5\%$, especially in the case of correlated impurities, are missing in Fig. S3(c).

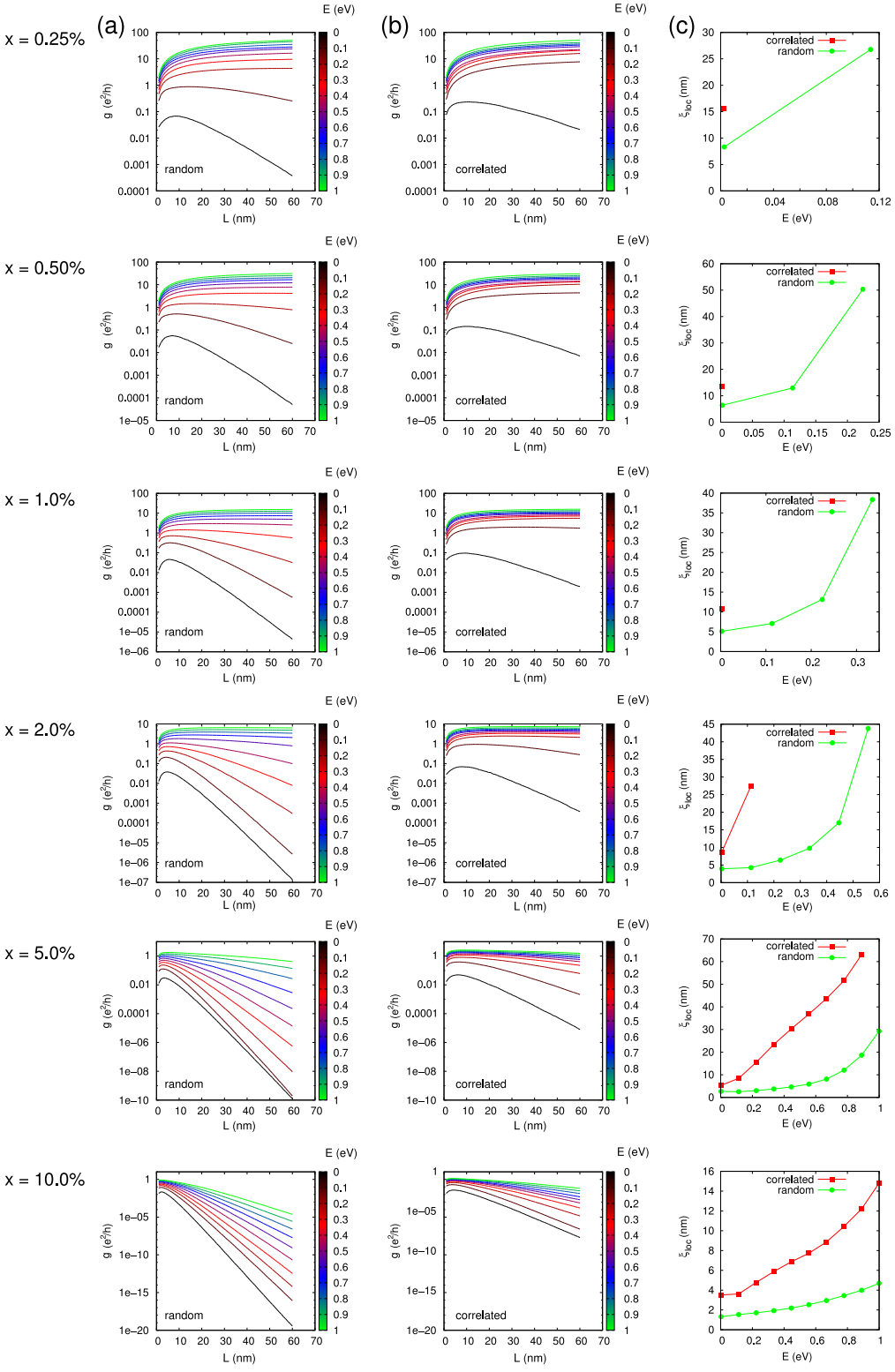

Figure S3: (Color online) Scaling analysis of conductivity g and localization length ξ_{loc} for concentrations $x = 0.25\%...10\%$. (a,b) Conductivity g as a function of scattering region length L calculated for graphene with random and correlated adatom distributions, respectively, at charge-carrier energies 0 eV $< E <$ 1 eV. (c) Localization length ξ_{loc} as a function of charge-carrier energy E for random and correlated adatom distributions.

E. Effect of the doping of leads in the Landauer-Büttiker calculations

Figure S4(a,b) shows the conductivity curves $g(L)$ for $x = 5\%$ concentration of randomly distributed adatoms obtained by shifting the charge neutrality point of leads by $\Delta E_{\rm L} = -0.5$ eV and $\Delta E_{\rm L} = -1.0$ eV, respectively. The effect of the doping of leads is two-fold. Firstly, the DOS of pristine graphene increases away from the charge neutrality point. Hence, upon doping the number of transport channels increases, which may result in larger values of conductance g. This is particularly important when the scattering region has an enhanced DOS at zero energy, such as graphene with resonant impurities. A comparison of Fig. S4(a) and Fig. S3(a) for $x = 5\%$ shows that conductivity is indeed enhanced at low energies with a crossing of the $g(L)$ curves at $L \approx 10$ nm. Secondly, doping results in a mismatch between the Fermi wavelength of the leads and that of the scattering region, which has a detrimental effect on conductance g. This effect is expected to be more pronounced at higher doping and high energy, where localization plays a smaller role. Indeed, at higher doping ($\Delta E_{\rm L} = -1.0$ eV) and high energy ($E = 1.0$ eV) the conductivity is reduced, notably at short distance $L < 10$ nm [Fig. S4(a,b)]. On the other hand, at large distances a general increase of the conductance is progressively restored since the conductivity becomes predominantly determined by the localization of the wavefunction and the increased number of available states. Finally, as shown in Fig. S4(c), localization length $\xi_{\rm loc}$ is practically unaffected by the doping of the leads, since it is an intrinsic property of the scattering region.

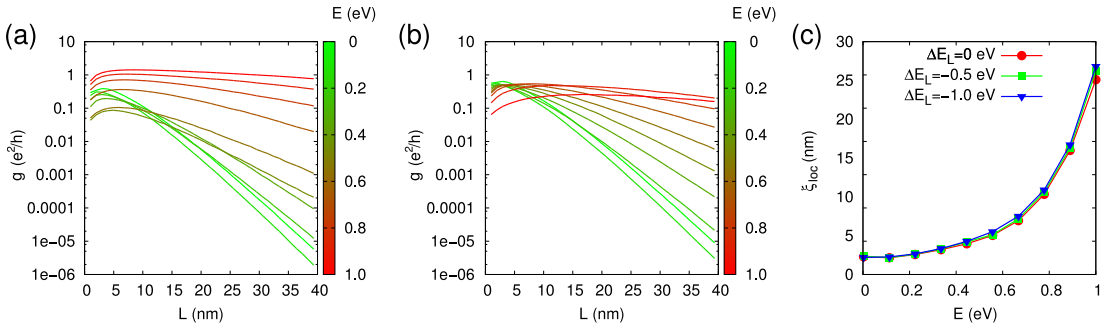

Figure S4: (Color online) (a,b) Conductivity g as a function of scattering region length L for graphene with randomly distributed adatoms at $x = 5\%$. The charge neutrality point of the leads has been shifted by (a) $\Delta E_{\rm L} = -0.5$ eV and (b) $\Delta E_{\rm L} = -1.0$ eV, respectively. (c) Localization length $\xi_{\rm loc}$ as a function of charge-carrier energy E for the two investigated lead doping levels compared to undoped leads $\Delta E_{\rm L} = 0$ eV.

F. Electronic transport calculations within the Kubo-Greenwood formalism using the kernel polynomial method

The diagonal elements of the real part of the frequency dependent conductivity tensor in linear response theory is given by the Kubo-Greenwood formula

$$Re\{\sigma_{\alpha\alpha}(\omega)\} = \frac{\pi}{V}\int dE \frac{f(E) - f(E+\hbar\omega)}{\omega} \times \mathrm{Tr}\{\delta(E-H)j_\alpha \delta(E-H+\hbar\omega)j_\alpha\}. \tag{8}$$

Here, $f(E)$ is the Fermi function and H the single-particle tight-binding Hamiltonian of the system under consideration, whereas the vectorial component of the current operator j_α is defined later. In the thermodynamic limit for zero temperature and zero frequency this equation reduces to

$$Re\{\sigma_{\alpha\alpha}(0)\} = \frac{\pi\hbar}{V}\mathrm{Tr}\{\delta(E_{\rm F}-H)j_\alpha \delta(E_{\rm F}-H)j_\alpha\}, \tag{9}$$

which defines the DC-conductivity studied in this work. The evaluation of this expression is carried out by employing the kernel polynomial method (KPM), as described in detail in Ref. 11. In this framework, the following matrix element density is defined

$$j(E,E') = \frac{1}{V}\sum_{n,m}\langle n|j_\alpha|m\rangle\langle m|j_\alpha|n\rangle \delta(E-\hbar\omega_n)\delta(E'-\hbar\omega_m), \tag{10}$$

which is then expanded up to finite order M within the two-dimensional KPM using the Jackson kernel. For the studied supercells containing up to $N_C \sim 10^6$ carbon atoms, we used $M = 1280$. The real-part of the frequency dependent conductivity tensor is then given by a double integration over the matrix density for arbitrary temperature and Fermi level:

$$Re\{\sigma_{\alpha\alpha}(\omega)\} = \frac{\pi}{\omega}\int_{-\infty}^{\infty} dE \int_{-\infty}^{\infty} dE' j(E,E') \times [f(E) - f(E')]\,\delta(\hbar\omega - (E' - E)). \tag{11}$$

As a result, the DC-conductivity can be expressed in terms of the diagonal elements of $j(E, E')$:

$$Re\{\sigma_{\alpha\alpha}(0)\} = \pi\hbar j(E_F, E_F). \tag{12}$$

The calculation of transport properties requires the definition of a current operator appropriate to the employed single-particle tight-binding model. Thus, we approximate the spatial operator r in a diagonal form:

$$r^\gamma \approx \sum_i r_i^\gamma c_i^\dagger c_i. \tag{13}$$

Consequently, one can derive the following current operator used in this work,

$$j_\gamma = -i\frac{e_0}{\hbar}\sum_{ij} t_{ij}(r_j^\gamma - r_i^\gamma)c_i^\dagger c_j, \tag{14}$$

where indices i and j run over atomic positions and γ denotes the vectorial component. For details of a similar derivation see e.g. Ref. 12.

G. Results for the calculations of conductivity using the kernel polynomial method

Figure S5(a,b) shows conductivity g as a function of charge-carrier energy E calculated using the KPM for random and correlated impurity distributions at two different adatom concentrations $x = 0.5\%$ and $x = 5.0\%$. A scaling

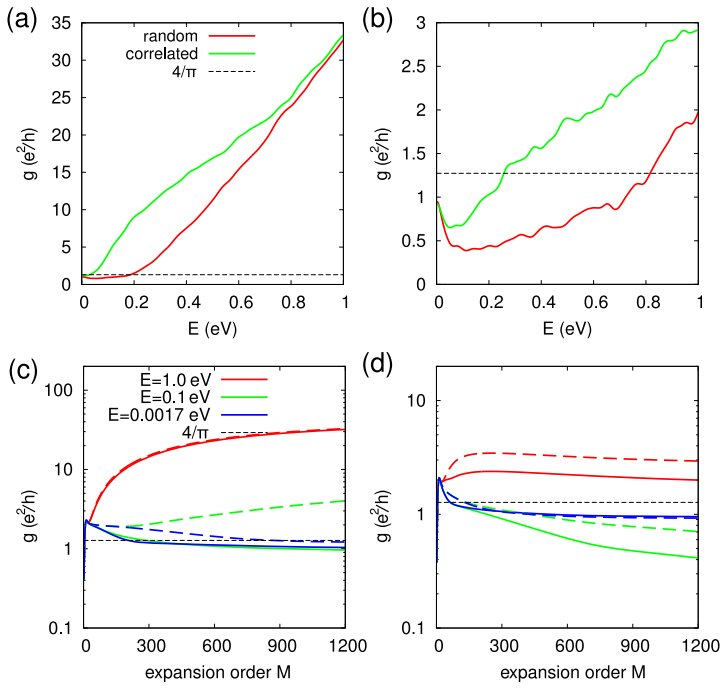

Figure S5: (Color online) (a,b) Conductivity g as a function of charge-carrier energy E calculated using the kernel polynomial method (KPM) for the random and correlated impurity distributions at $x = 0.5\%$ and $x = 5.0\%$ adatom concentrations, respectively. (c,d) Conductivity g as a function of expansion order M for the random and correlated impurity distributions at $x = 0.5\%$ and $x = 5.0\%$ adatom concentrations, respectively. The dashed lines indicate the minimum conductivity of graphene.

analysis of the conductivity for three charge carrier energies ($E = 1.7 \times 10^{-3}$ eV, $E = 0.1$ eV and $E = 1.0$ eV) based on the expansion order M is shown in Fig. S5(c,d) for the same values of adatom concentration x. The order M relates to a timescale $\tau(M)$ [13]. For $E = 1.0$ eV and $x = 5\%$ the conductivity rises with increasing expansion order M, exhibits a maximum around $M \sim 200$ and then decreases slowly again for both correlated (dashed line) and random (solid line) impurity distributions [Fig. S5(d)]. We interpret these maxima as the semiclassical values of conductivity g_{sc} corresponding to the diffusive regime, followed by quantum corrections which result in the decrease of the conductivity. For a concentration of $x = 0.5\%$ and $E = 1.0$ eV no conductivity maximum is observed, which indicates that the results still correspond to the pre-diffusive/ballistic regime for the largest expansion order investigated. A shift of g_{sc} to larger expansion orders for decreasing x is expected, because fewer scattering centers are present. The situation is, in general, different for small energies close to the Dirac point (here, $E = 1.7 \times 10^{-3}$ eV), in both cases of correlated and random adatom distributions as well as concentrations of $x = 0.5\%$ and $x = 5\%$. A distinct maximum for $M > 100$ is completely absent, and only a reduction of the conductivity is observed for increasing M. Thus, we relate this characteristic to the quantum regime with localization effects resulting in a reduced localization length. If the expansion order is sufficiently large, the curves for $E = 1.7 \times 10^{-3}$ eV reach values well below $g = 4/\pi(e^2/h)$, and one may expect the conductivity to converge asymptotically to zero in the limit of $M \to \infty$ if the modes are completely localized.

[1] J. P. Perdew, K. Burke, and M. Ernzerhof, Phys. Rev. Lett. **77**, 3865 (1996).
[2] D. Vanderbilt, Phys. Rev. B **41**, 7892 (1990).
[3] H. J. Monkhorst and J. D. Pack, Phys. Rev. B **13**, 5188 (1976).
[4] P. Giannozzi, S. Baroni, N. Bonini, M. Calandra, R. Car, C. Cavazzoni, D. Ceresoli, G. L. Chiarotti, M. Cococcioni, I. Dabo, A. D. Corso, S. d. Gironcoli, S. Fabris, G. Fratesi, R. Gebauer, U. Gerstmann, C. Gougoussis, A. Kokalj, M. Lazzeri, L. Martin-Samos, N. Marzari, F. Mauri, R. Mazzarello, S. Paolini, A. Pasquarello, L. Paulatto, C. Sbraccia, S. Scandolo, G. Sclauzero, A. P. Seitsonen, A. Smogunov, P. Umari, and R. M. Wentzcovitch, J. Phys.: Condens. Matt. **21**, 395502 (2009).
[5] Y. Lin, F. Ding, and B. I. Yakobson, Phys. Rev. B **78**, 041402 (2008).
[6] D. W. Boukhvalov, M. I. Katsnelson, and A. I. Lichtenstein, Phys. Rev. B **77**, 035427 (2008).
[7] M. Büttiker, Y. Imry, R. Landauer, and S. Pinhas, Phys. Rev. B **31**, 6207 (1985).
[8] J. Mathon and A. Umerski, Phys. Rev. B **63**, 220403 (2001).
[9] A. Umerski, Phys. Rev. B **55**, 5266 (1997).
[10] S. Sanvito, C. J. Lambert, J. H. Jefferson, and A. M. Bratkovsky, Phys. Rev. B **59**, 11936 (1999).
[11] A. Weiße, G. Wellein, A. Alvermann, and H. Fehske, Rev. Mod. Phys. **78**, 275 (2006).
[12] J. M. Tomczak and S. Biermann, Phys. Rev. B **80**, 085117 (2009).
[13] S. Roche, Phys. Rev. B **59**, 2284 (1999).